Heat and Mass Transfer 40 (2003) 105–114
DOI 10.1007/s00231-002-0373-0

Soret effect and slow mass diffusion as a catalyst for overstability in Marangoni-Bénard flows

A. Bergeon, R. Mollaret, D. Henry

Abstract We study the onset of time dependent Marangoni-Bénard convection in binary mixtures subject to Soret effect by numerical computation of linear instability thresholds in infinite fluid layers and two-dimensional boxes. The calculations are done for positive Marangoni numbers ($Ma > 0$) and negative Marangoni Soret parameters $S_M = -(D_S\gamma_c)/(D\gamma_T)$ where D_S and D are the Soret and mass diffusion coefficients, respectively, and γ_T, γ_c are the first derivatives of the surface tension with respect to temperature and concentration. Our purpose is to understand why for particular choices of Prandtl and Schmidt numbers, the increase of the stabilizing solutal contribution leads to a decrease of the critical temperature difference, a phenomenon already reported by Chen & Chen [5] and Skarda et al. [12] For various choices of Prandtl and Schmidt numbers we analyze the evolution of the critical Marangoni number Ma_c, critical wavenumber k_c and angular frequency ω_c with S_M and compute the corresponding eigenvectors. We next propose a physical mechanism which explains how the stabilizing solutal contribution acts as a catalyst for overstability. Finally, we extend our results to two dimensional boxes of small aspect ratio.

1 Introduction

Flows induced by surface tension effects arise in many industrial process with a contact surface between a liquid and a gas or two immiscible fluids. When surface tension gradients are created by variations of temperature along the interface, the induced convective flows are called Marangoni convection and when the applied temperature gradient is perpendicular to the interface, it is called Marangoni-Bénard convection.

It is known that gravity plays an important role in the obtained microstructures developed during solidification processes by influencing the melt in the liquid phase. With the near elimination of buoyancy forces, microgravity provides apparently a promising environment for material processing. But if on earth, thermocapillay effects on convection are generally overshadowed by buoyancy forces, in microgravity they predominate and particularly in floating zone configurations. Since the quality of the material depends strongly on the concentration distribution in the liquid phase, it is necessary to understand and control the onset of Marangoni convection. The configurations that we study are close to those arising in the floating zone technique. In the present paper, we study the combined influence of temperature and concentration on the onset of time-periodic Marangoni-Bénard motions in the absence of gravity.

In microgravity conditions, an initial species separation is induced via the Soret effect by the imposed temperature gradient. The Soret-induced solute flux has a stabilizing or destabilizing effect on the diffusive state depending on the relative variations of the surface tension with the temperature and concentration. Their relative influence is contained in the signs of the Marangoni number Ma and the Soret coupling coefficient S_M (called hereafter the Marangoni Soret parameter).

The linear stability analysis of this problem has been studied in various configurations including two-dimensional boxes or layers of infinite horizontal extension with a flat or deformed free surface [1–13]. The results of the linear stability are summarized in a graph presenting the critical Marangoni number Ma_c versus the Marangoni Soret parameter S_M. At $S_M = 0$, there is no induced species separation so that the situation is the one studied by Pearson [14] in an infinite layer. We refer to the case $S_M = 0$ as the pure thermal case. In the parameter space (S_M, Ma), convection may appear in three of the four quadrants. If both Ma and S_M are positive, thermal and solutal contributions to the surface force are destabilizing and the threshold Ma_c decreases with S_M. On the other hand, the critical size of the convective rolls increases and for sufficiently large S_M single roll flow structures are observed right above the threshold of a bounded box. If both Ma and S_M are negative, only the solutal contribution is destabilizing. In this case and over the whole quadrant, the critical wavenumber is zero and in bounded boxes, one-roll flows bifurcate from the first threshold Ma_c. In those two quadrants, steady flows are predicted and observed numerically.

In the present work, we study situations with negative Marangoni Soret parameters and positive Marangoni

Received: 11 February 2002
Published online: 12 October 2002

A. Bergeon (✉), R. Mollaret
Université P. Sabatier/IMFT U.M.R. C.N.R.S.
5502, Dépt. Mécanique Bat. 1R2, 118, route de Narbonne,
31062 Toulouse Cedex, France
E-mail: bergeon@im2f.ups-tlse.fr

D. Henry
U.M.R. C.N.R.S. 5509, LMFA-ECL-UCB, ECL,
BP 163, 69131 Ecully Cedex, France

numbers. In this range of parameters, the solutal contribution to the free surface force is stabilizing and the thermal contribution destabilizing. The stabilizing solutal effect increases as S_M becomes more negative so that the critical Marangoni number at which steady states bifurcate increases with $|S_M|$ [3, 5, 6, 9, 12]. Below a particular Marangoni Soret parameter, the first bifurcation to a steady state is replaced by a Hopf bifurcation creating time periodic motions [5, 7, 12].

The variations of the Hopf critical Marangoni number with S_M depend strongly on the Prandtl and Lewis numbers. Bhattacharjee [6] calculated analytically the curves $Ma_c(S_M)$ for negative S_M allowing the interface to be deformed by the flow. For a flat free surface, his results for large Lewis numbers Le (here $Le = \kappa/D$ where κ is the thermal diffusivity and D the mass diffusion coefficient) and large Prandtl numbers Pr ($Pr = \nu/\kappa$ where ν is the kinematic viscosity) indicate that Ma_c increases as S_M becomes more negative. In contrast, the numerical results of Chen & Chen [5] for large Lewis numbers ($Le = 100$ and $Pr = 7$) show that Ma_c first decreases as S_M becomes more negative. This behavior, originally reported by Castillo & Velarde [1], is also observed in the analytical linear stability analysis of Skarda et al. [12].

Our objective is to draw a link between these two types of behaviors and propose a physical interpretation. We mention that the decrease of Ma_c with $|S_M|$ is surprising since one would expect an increase of the threshold as the result of an increasing stabilizing effect. To understand this effect, we analyze the influence of the Prandtl and Schmidt numbers on the onset of convection before proposing a physical mechanism. For that, the linear problem for the primary Hopf bifurcation is formulated and solved numerically. The scaled equations and numerical methods are outlined in the next section. The last section presents the results in the case of an infinite fluid layer and in the case of a two-dimensional box.

2
Linear problem and numerical methods

In the present section, we describe the dimensionless linear problem and the numerical method used to compute the Hopf bifurcation points. The same method (namely a Newton method) is applied to boxes of finite extension and to infinite layers. The first subsection presents the system of equations that we have to solve in a two-dimensional box. The next two subsections describe the numerical procedure used to solve the problem in a bounded box and in a layer of infinite horizontal extent. This is followed by a subsection in which we discuss the accuracy of the results.

2.1
Dimensionless linear problem

We consider a non-reactive binary fluid layer confined in an open cavity of length L in the horizontal and height H in the vertical. The box is open and the upper boundary is a free surface heated by a constant and normal heat flux $\mathbf{q} = -q\mathbf{z}$ (with $q > 0$ and $\mathbf{z}$ an upwards unit vector, normal to the free surface) while the lower rigid boundary is maintained at a constant temperature T_0. The free surface is assumed to be flat and subject to surface tension.

We assume that the surface tension σ varies linearly with the temperature T and the mass fraction c,

$$\sigma(T, c) = \sigma_0 + \gamma_T(T - T_0) + \gamma_c(c - c_0), \tag{1}$$

where γ_T and γ_c are the derivatives of the surface tension with respect to T and c, respectively, and c_0 is the initial solute mass-fraction. The fluid mixture is subject to the Soret effect and the mass flux is thus a linear combination of the temperature and concentration gradients. Neglecting the Dufour effect [15], the fluxes are:

$$\mathbf{J}_c = -\rho D\nabla c - \rho D_S\nabla T, \tag{2}$$

$$\mathbf{J}_T = -\lambda\nabla T, \tag{3}$$

where λ is the thermal conductivity, D the mass diffusion coefficient, and D_S is the Soret diffusion coefficient. We mention that the Soret effect is often described in terms of the separation ratio $D_S/D = \pm S_T\bar{c}(1 - \bar{c})$ where S_T is called the Soret coefficient and $\bar{c}$ is taken to be the mean solute concentration within the layer [5]. Despite the fact that the value and the sign of S_T depend on the mean solute concentration [16] we assume here that D_S is constant.

We recall that the gravity level is zero. 'No-slip' conditions are imposed along the rigid boundaries and the normal mass flux is zero across all the boundaries. The stress balance along the free surface reads,

$$\mu\frac{\partial u}{\partial z} = \frac{\partial\sigma}{\partial x}, \tag{4}$$

where u is the horizontal component of the velocity field $\mathbf{u} = (u,w)$ and μ is the dynamic viscosity. The problem has the following trivial steady solution:

$$u = w = 0 \quad T = T_0 + \frac{\Delta T}{H}\left(z - \frac{H}{2}\right) \quad c = c_0 + \frac{\Delta c}{H}\left(z - \frac{H}{2}\right) \tag{5}$$

where H is the depth of the layer. $\Delta T = +qH/\lambda$ is the temperature difference resulting from the constant heat flux applied on the free surface when diffusion is well established. $\Delta c = -D_S\Delta T/D$ is the concentration difference obtained at the Soret conductive state as the result of the applied temperature difference.

The equations are scaled using H, H^2/ν, $Ma\ \nu/H$, ΔT and Δc for distance, time, velocity, temperature and concentration, respectively, where ν is the kinematic viscosity. In the following, the variables (u, w, p, T, c) then refer to dimensionless velocity, pressure, temperature and concentration. The conductive state now reads $u = w = 0$, $T = c = z - 0.5$. Let us denote $\mathbf{U} = (\mathbf{u}, p, T, c)$ the conductive state and $\mathbf{U}' = (\mathbf{u}', p', T', c')$ perturbations of this solution. Linearizing about the conductive solution $\mathbf{U}$ gives the following set of equations:

$$\frac{\partial\mathbf{u}'}{\partial t} = \nabla^2\mathbf{u}' = \nabla p', \tag{6}$$

$$\frac{\partial T'}{\partial t} = -Ma\,w' + \frac{1}{Pr}\nabla^2 T', \tag{7}$$

$$\frac{\partial c'}{\partial t} = -Ma\, w' \frac{1}{Sc}(\nabla^2 c' - \nabla^2 T'), \tag{8}$$

$$0 = \nabla \cdot \mathbf{u}', \tag{9}$$

with the boundary conditions:

$$\text{along } z = 0, \quad u' = w' = 0 \quad T' = 0 \quad \frac{\partial c'}{\partial z} = \frac{\partial T'}{\partial z}, \tag{10}$$

$$\text{along } z = 1, \quad \frac{\partial u'}{\partial z} - \frac{1}{Pr}\left(\frac{\partial T'}{\partial x} + S_M \frac{\partial c'}{\partial x}\right) = w' = \frac{\partial T'}{\partial z} = \frac{\partial c'}{\partial z} = 0, \tag{11}$$

$$\text{along } x = 0 \text{ and } x = A, \quad u' = w' = \frac{\partial T'}{\partial x} = \frac{\partial c'}{\partial x} = 0. \tag{12}$$

where $A = L/H$ is the aspect ratio of the box, Pr and Sc are the Prandtl and the Schmidt numbers, respectively, and Ma is the Marangoni number defined by:

$$Ma = \frac{\Delta T H \gamma_T}{\rho \nu \kappa}. \tag{13}$$

S_M is what we call the Marangoni Soret parameter and represents the ratio of the solutal contribution to the thermal contribution to the surface force and is defined by:

$$S_M = -\frac{D_S \gamma_c}{D \gamma_T}. \tag{14}$$

We mention that our choice of dimensionless numbers is consistent with the one used by Skarda et al. [12] (the stability is discussed with respect to $S_m = -S_M$) but differs from Chen & Chen [5].

2.2 Numerical method

We can write the perturbations as $\mathbf{U}' = (u'(x, z, t), w'(x, z, t), p'(x, z, t), T'(x, z, t), c'(x, z, t))$. Let us rewrite equations (6–12) in the following abbreviated form:

$$\frac{\partial \mathbf{U}'}{\partial t} = J_{Ma}\mathbf{U}' \quad \text{in } \Omega =]0, A[\times]0, 1[, \tag{15}$$

$$B\mathbf{U}' = 0 \quad \text{in } \partial\Omega \cup \Omega, \tag{16}$$

where J_{Ma} is a linear differential operator whose coefficients depend on Ma, and $B\mathbf{U}' = 0$ a linear equation expressing the linearized boundary conditions and the divergence free condition. For simplicity of the presentation, we omit equation (16) in the following. Time dependence of the perturbation is assumed to be of the form $\exp(\lambda t)$ so that the linearized problem is reduced to an eigenvalue problem. Let us denote $\mathbf{h} = \mathbf{h}_r + i\mathbf{h}_i$ the eigenvector associated to a purely imaginary eigenvalue $\lambda = i\omega_c$ and to the critical Marangoni number Ma_c. The problem reduces to:

$$i\omega_c \mathbf{h} = J_{Ma_c}\mathbf{h}, \tag{17}$$

where $\omega_c = 2\pi f_c$ and f_c is the critical frequency at the onset of convection. We rewrite this problem in the abbreviated real form:

$$\mathbf{f}(\mathbf{h}_r, \mathbf{h}_i, Ma_c, \omega_c) = \mathbf{f}(\mathbf{X}_c) = 0, \tag{18}$$

where $\mathbf{f}$ is a non-linear operator on $\mathbf{X}_c$ due to cross-products of Ma and ω with $\mathbf{h}_r$ and $\mathbf{h}_i$. We solve this non-linear set of equations by means of a Newton method [17]. At each Newton iteration, the linear differential equations that we have to solve are obtained by differentiating relation (18) with respect to the current estimate of the unknowns, the real and imaginary parts of the eigenvector, Ma and ω. Observing that $\mathbf{f}$ is a linear function of $(\mathbf{h}_r, \mathbf{h}_i)^T$, we get:

$$\begin{aligned}\mathbf{f}(\mathbf{d}h_r, \mathbf{d}h_i, Ma, \omega) + dMaD_{Ma}\mathbf{f}(\mathbf{h}_r, \mathbf{h}_i, Ma, \omega) \\ + d\omega D_\omega \mathbf{f}(\mathbf{h}_r, \mathbf{h}_i, Ma, \omega) = -\mathbf{f}(\mathbf{h}_r, \mathbf{h}_i, Ma, \omega),\end{aligned} \tag{19}$$

where $(\mathbf{d}h_r, \mathbf{d}h_i, dMa, d\omega)^T$ is the increment and D denotes differentiation. The system (19) is discretized by means of a pseudo-spectral method using Chebyschev polynomials [18, 19]. The discretized version of the linear system (19) consists of $N = 10 \times N_x \times N_z$ equations for the real and imaginary parts of the two velocity components, pressure, temperature and concentration at the $N_x \times N_z$ Gauss-Lobatto points [22]. The solution is $(\mathbf{d}h_r, \mathbf{d}h_i, dMa, d\omega)^T \in \mathrm{R}^{N+2}$. Therefore, in order to solve the linear system and by the way, exclude the trivial solution $\mathbf{h}_r = \mathbf{h}_i = \mathbf{0}$, we impose the requirement that a component of $\mathbf{h}_r$ and $\mathbf{h}_i$ is arbitrarily fixed at non-zero values during the Newton iterations:

$$(\mathbf{h}_r)_l = K_r \quad (\mathbf{h}_i)_m = K_i, \tag{20}$$

which gives, after differentiation, $(\mathbf{d}h_r)_l = (\mathbf{d}h_i)_m = 0$.

Recall that we have omitted to discuss the boundary conditions. These are in fact included into the discretized version of the linear system (19). For instance, the linearized equation for the temperature along the bottom of the box, $T = 0$, gives the Newton system $dT = -T$. The lines of the system (19) corresponding to the unknowns involved in this condition are replaced by the discretized version of this equation [17]. The convergence of the Newton method is obtained when $||\mathbf{f}(\mathbf{h}_r, \mathbf{h}_i, Ma, \omega)|| < \epsilon$ with $\epsilon = 10^{-7}$.

2.3 Infinite layer

For a horizontally infinite layer, we replace the boundary conditions at the lateral walls by periodic boundary conditions with imposed wavenumber k. We seek Hopf bifurcations and expand the variables (u', w', p', T', c') as $(u^\star(z), w^\star(z), p^\star(z), T^\star(z), c^\star(z)) \cdot \exp(i(\omega t + kx))$. The functions $(u^\star(z), w^\star(z), p^\star(z), T^\star(z), c^\star(z))$ are complex. The resulting set of equations is described in the appendix A. We note that it is non-linear with respect to the variables $(u^\star, w^\star, p^\star, T^\star, c^\star, Ma, \omega)$. To obtain the critical Marangoni number, we fix the physical properties (Pr, Sc, S_M) and we solve the system for various values of k. We obtain $Ma(k)$ and $\omega(k)$. The critical Marangoni number Ma_c is the smallest value of $Ma(k)$ ($Ma_c = \min_{k>0} Ma(k) = Ma(k_c)$) and the critical frequency is $\omega_c = \omega(k_c)$. At a steady bifurcation, $\omega_c = 0$ and the flow structure of the critical eigenmode corresponds to the real part of $(u^\star(z), w^\star(z), p^\star(z), T^\star(z), c^\star(z)) \exp(ik_c x)$ which is: $\mathbf{h}_c = \mathbf{h}_r \cos k_c x - \mathbf{h}_i \sin k_c x$. At a Hopf bifurcation point, $\omega_c \neq 0$ and the flow structure close to the onset of instability is the real part of $(u^\star(z), w^\star(z), p^\star(z), T^\star(z), c^\star(z)) \exp(i(k_c x + \omega_c t))$

that is $\mathbf{h}_c = \mathbf{h}_r \cos(k_c x + \omega_c t) - \mathbf{h}_i \sin(k_c x + \omega_c t)$. The resolution chosen for the calculations concerning the infinite layer is $N_z = 19$.

2.4 Accuracy

The above method for an infinite layer does not exclude primary steady bifurcation points. For such points, solutions verify $\omega_c = 0$ and $\mathbf{h}_r$ is proportional to $\mathbf{h}_i$. First, we have checked the accuracy of the code on the analytical results of Pearson for an infinite layer of a one component fluid. We obtained $Ma_c = 79.6067$ with $N_z = 19$ a result which is accurate to the third decimal. Finally, we checked our code on the results presented in [5, 12] for Hopf bifurcations.

As no quantitative results were available in the literature for Hopf primary bifurcation points in bounded boxes, we checked the accuracy of the numerical code in this case on the results of Bergeon et al. [9, 11] for steady primary bifurcation points. The method they used is also a Newton method but the Jacobian matrix is not explicitly computed. This matrix is in fact preconditioned by a time-step Δt dependent matrix $P_{\Delta t}$ so that the action of $P_{\Delta t} J_{Ma}$ on a vector can be computed efficiently by adapting a time-stepping code as described in [24, 25]. Table 1 displays the results of our comparison for a cavity with aspect ratio $A = 2$ and a fluid with $Sc = 60$, $Pr = 0.6$ and $S_M = 0$. Different grids have been used which proves the good agreement between the two methods.

The self-consistency of the method has been checked for $S_M \neq 0$ ($S_M = -0.001$) with variable grids (Table 2). Results show that for $A = 2$, $Sc = 100$ and $Pr = 1$, 15×13 points give results accurate to the fourth decimal for the critical period and Marangoni number. This last result has been compared to the critical values obtained by computing the leading eigenvalues of the Jacobian matrix using the Arnoldi method described by Tuckerman [20, 21]. These critical values are $Ma_c = 93.96$ with $\omega_c = 0.123$ for a grid 13×11, in good agreement with those found with the present method.

Table 1. Comparison of the first critical Marangoni number obtained in the present paper with the values obtained by Bergeon et al. [10, 12]. The situation is a cavity with aspect ratio $A = 2$ in the pure thermal situation for which the threshold value does not depend on the Prandtl number

$N_x \times N_z$	Ma_c (present work)	Ma_c (Bergeon et al. [9, 11])
11×11	93.0728	93.1407
13×11	93.0760	93.0847
15×13	93.0765	93.0779
19×15	93.0765	93.0765

Table 2. Evolution of the critical Marangoni number, corresponding pulsation and period T_t with the number of collocation points. The situation is a cavity with aspect ratio $A = 2$ with $Pr = 1$, $Sc = 100$ and $S_M = -0.001$

$N_x \times N_z$	Ma_c	ω_c	$T_{t,\,c}$
11×11	93.9657	0.129352	48.5743
13×11	93.9691	0.129356	48.5728
15×13	93.9695	0.129357	48.5724
19×15	93.9696	0.129357	48.5724

3 Results

We recall that, in the present work, S_M is always negative, so that we will discuss the relative influence of the thermal and solutal surface forces in terms of $|S_M|$. We will mainly discuss the case of an infinite layer, before presenting some results for bounded boxes in the last subsection.

3.1 The global picture

Figure 1 displays for an infinite layer, the evolution of the critical Marangoni number Ma_c, the critical wavenumber k_c, and the critical angular frequency ω_c with the Marangoni Soret parameter S_M for a fixed Lewis number $Le = Sc/Pr = 100$ and three choices of (Pr, Sc).

For slightly negative Marangoni Soret parameters, the first bifurcation is steady ($\omega_c = 0$) and the corresponding critical Marangoni number increases towards infinity as $|S_M|$ increases. At a negative value $S_M = S_{M_T}$ the curves of

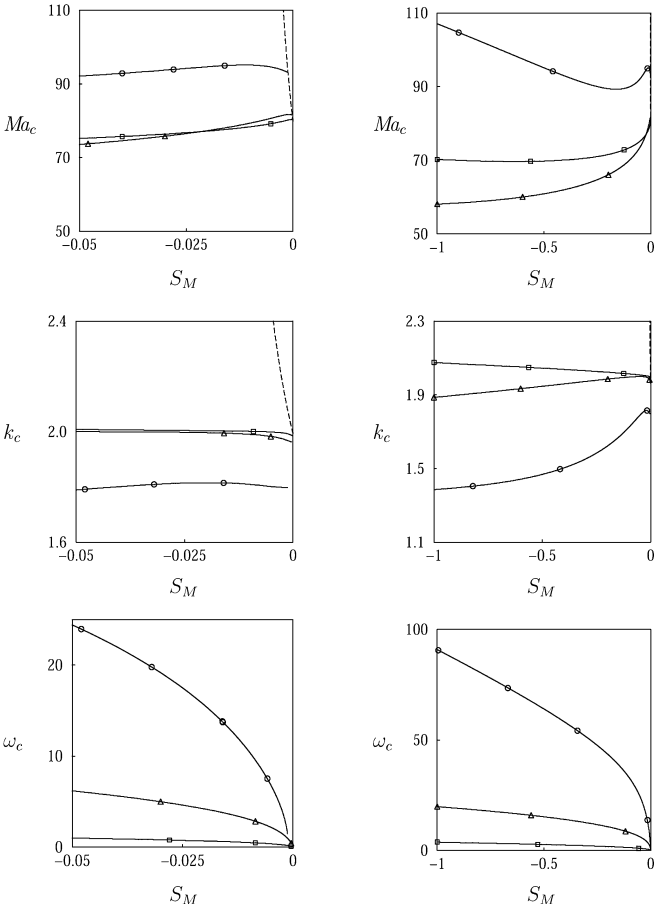

Fig. 1. Evolution of the critical Marangoni number Ma_c (on top), critical wavenumber k_c and critical pulsation ω_c with the Marangoni Soret parameter S_M for a Lewis number $Le = 100$. Squares correspond to $Pr = 1$ and $Sc = 100$, triangles to $Pr = 0.1$ and $Sc = 10$ and circles to $Pr = 0.01$, $Sc = 1$

Hopf and steady bifurcations intersect. The value S_{M_T} depends on (Pr, Sc) separately and thus S_{M_T} differs for the three curves. More precisely, the curve $Ma_c(S_M)$ associated to steady bifurcations goes to infinity as S_M approaches from above a particular value $S_{M_A} < S_{M_T}$.

The value S_{M_A} has been calculated analytically by Bhattacharjee [6] as a function of Le and he obtained $Ma_c = Ma_0/(1 + \psi(1 + 1/L))$ with $S_M = \psi$ and $L = 1/Le$. His result can be recovered using simple arguments as follow. For steady bifurcations, the changes of variables $T'' = T'/Pr$, $\mathbf{u}'' = Ma\mathbf{u}'$ and $C'' = (C' - T')/Sc$ lead to similar evolution equations for T'' and C'' (the only difference coming from the boundary conditions at the bottom) and indicate that the magnitude of the gradients of the temperature and concentration perturbations are of the same order. The dimensionless parameters reduce to $\overline{\mathrm{Ma}} = \mathrm{Ma}(1 + \mathrm{S\_M})$ and $\psi_M = S_M Le/(S_M + 1)$ which only appear in the stress equilibrium at the free surface through the relation $\partial u''/\partial z = F_T \partial T''/\partial x + F_c \partial c''/\partial x$ with $F_T = \overline{Ma}$ and $F_c = \overline{Ma}\psi_M$. F_T and F_c represent the magnitudes of the thermal and solutal surface forces respectively. For $S_M = 0$, convection occurs if the magnitude of the thermal force exceeds the critical Marangoni number Ma_0 of the pure thermal situation. Here, with the additional solutal contribution, the total force $F_T + F_c$ must now exceed Ma_0 and this leads to: $Ma_c \approx Ma_0/(1 + S_M(1 + Le))$. This value (the same as the one of Bhattacharjee [6]) indicates that the critical Marangoni number decreases as S_M increases and that Ma_c increases to infinity as S_M decreases to $S_{M_A} = -1/(Le + 1)$. The exact location of the asymptote is discussed in [12] for various thermal boundary conditions.

For $S_M < S_{M_T}$, the first bifurcation is a Hopf bifurcation. For S_M smaller than but close to S_{M_T}, the critical Marangoni number of overstability first increases with $|S_M|$ and then decreases for larger $|S_M|$. This particular feature already observed by [5, 12] is surprising since the increase of $|S_M|$ corresponds to an increase of the stabilizing solutal contribution to the surface force. Moreover, figure 1 indicates that the critical Marangoni number may pass below the critical value obtained in the pure thermal situation, $Ma_0 \approx 80$ [14]. The curve $Ma_c(S_M)$ corresponding to $Pr = 0.01$ and $Sc = 1$ finally increases at larger $|S_M|$. We also observed this behaviour on the two other curves of figure 1 for Marangoni Soret parameters $S_M > -1$.

We also note that at the intersection with the steady bifurcation curve (at $S_M = S_{M_T}$), the critical angular frequency for the Hopf bifurcation does not correspond to $\omega_c = 0$ and that there is a gap between the critical wavenumber of the steady bifurcation and that of the Hopf bifurcation. Consequently and according to Knobloch & Moore [22], we slightly disagree with Chen & Chen [5] and Skarda et al. [12] who refer to the junction of the steady and Hopf bifurcation curve at S_{M_T} as a codimension-two bifurcation point. More precisely, Knobloch & Moore [22] note that the codimension-two bifurcation point (characterized by the infinite period $\omega_c = 0$) can be observed in sufficiently small aspect ratio boxes but not in infinite layers for which there is no geometrical constraint on the flow.

3.2
Influence of *Pr*, *Sc* and S_M on the Hopf bifurcation

In this problem, there are three parameters on which the critical Marangoni number, wavenumber and pulsation depend: the Prandtl and the Schmidt numbers, Pr and Sc, and the Marangoni Soret parameter S_M. In the following, we study the influence of Pr and Sc on the evolution of Ma_c with S_M. Different choices of Pr and Sc corresponding to different fluids will be discussed. For instance, $Pr \approx 10$ and $Sc \approx 100$ correspond to aqueous solutions [5], $Pr \approx 1$ and $Sc \approx 10$–100 to molten salts [23] and $Pr \approx 0.01$ and $Sc \approx 100$ to molten metals.

In figure 2 we present the critical Marangoni number, wavenumber, and angular frequency versus the Marangoni Soret parameter for a fixed Schmidt number $Sc = 100$ and various Prandtl numbers $Pr = 0.1$, 1 and 10. The critical values are presented in figure 3 but for a fixed Prandtl number $Pr = 0.1$ and various Schmidt numbers $Sc = 1$, 10 and 100.

Figures 2 and 3 show that in all cases, the critical angular frequency increases with the absolute value of the Marangoni Soret parameter. The influences of Pr and Sc are not so clear, but for sufficiently large values of $|S_M|$, the critical angular frequency decreases as Pr and Sc increase. Concerning k_c, figures 1, 2, and 3 indicate that the

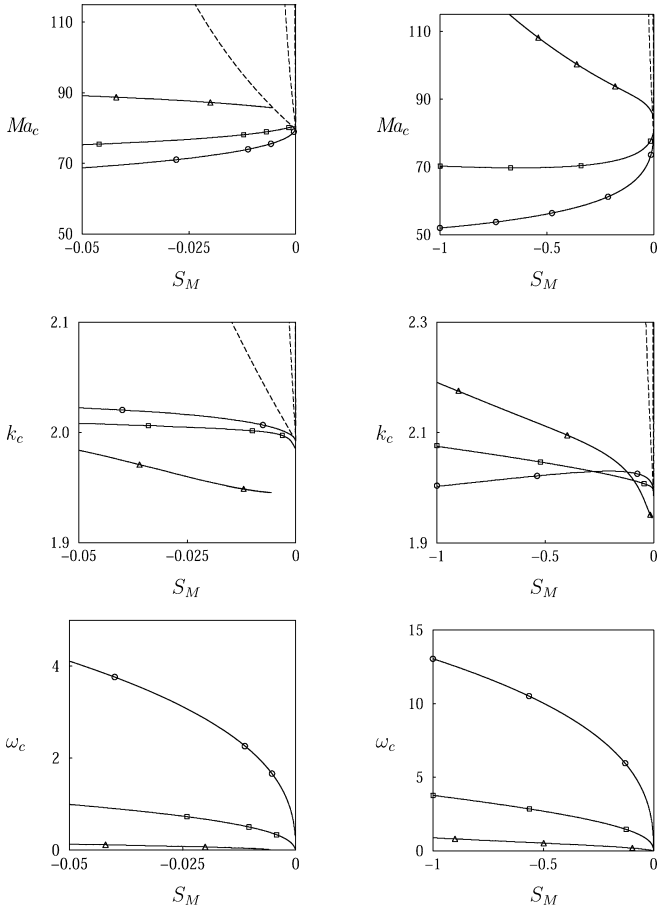

Fig. 2. Evolution of the critical Marangoni number Ma_c (on top), critical wavenumber k_c and critical pulsation ω_c with the Marangoni Soret parameter S_M for $Sc = 100$. Triangles correspond to $Pr = 10$, squares to $Pr = 1$ and circles to $Pr = 0.1$

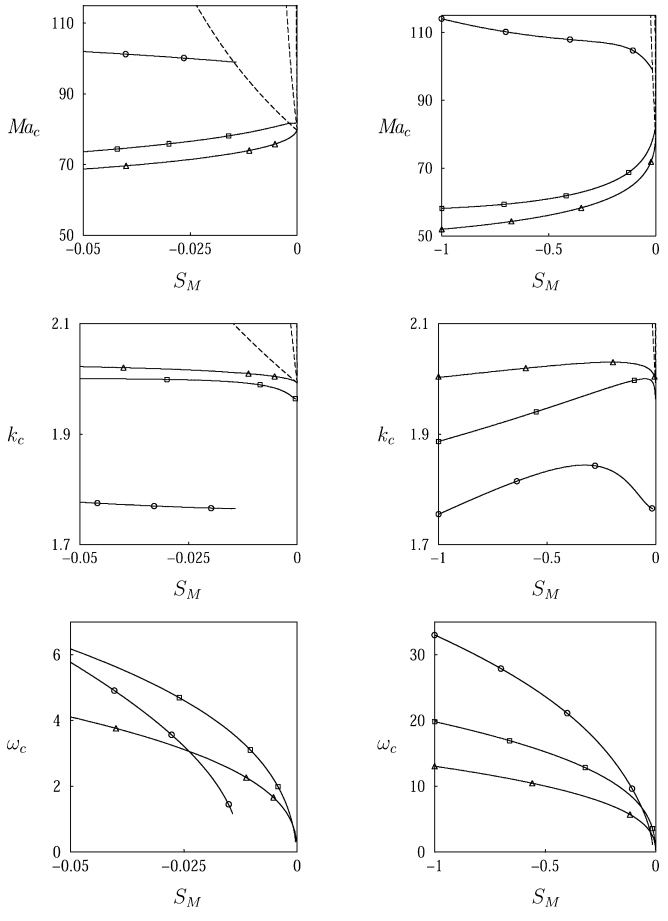

Fig. 3. Evolution of the critical Marangoni number Ma_c (on top), critical wavenumber k_c and critical pulsation ω_c with the Marangoni Soret parameter S_M for $Pr = 0.1$. Triangles correspond to $Sc = 100$, squares to $Sc = 10$ and circles to $Sc = 1$

variations of k_c with $|S_M|$ can be characterized in most cases and after a region close to $S_{M,T}$ ($S_M \lessapprox S_{M,T}$), by an almost linear evolution (increase or decrease of k_c with $|S_M|$). For $|S_M|$ sufficiently large, figure 2 and 3 show that k_c increases with Pr or Sc. This increase is stronger when the increases of Pr and Sc are combined as in figure 1. Nevertheless, in most cases, the variations of k_c are not very large, and the values remain around 2.

Examination of Figures 2 and 3 also give indications on the variations with Sc and Pr of the discontinuities of ω_c and k_c at $S_M = S_{M_T}$: for decreasing Sc, both discontinuities increase. As mentioned by Bhattacharjee [6], S_{M_T} is a codimension-two bifurcation point in the limit where $Sc \to \infty$.

The structures of the eigenflows are presented in figures 4 and 5 through isovalues of the streamfunction, temperature and concentration for different Lewis numbers, for S_M close to S_{M_T} (figure 4) and for $S_M = -0.5$ (figure 5). To evaluate the streamfunction ϕ at an instant t, we state that it is solution of $\partial\phi/\partial z = \text{real}(u(t)) = u_r \cos(k_c x + \omega_c t) - u_i \sin(k_c x + \omega_c t)$ and $\partial\phi/\partial x = -\text{real}(w(t)) = -(w_r \cos(k_c x + \omega_c t) - w_i \sin(k_c x + \omega_c t))$, where u, w are complex functions, and u_r, w_r, u_i, w_i real functions of z. Solving these equations for ϕ with the use of the continuity constraint ($k_c u_r + w'_i = -k_c u_i + w'_r = 0$) leads to: $\phi(x, z, t) = -(1/k_c)(w_r \sin(k_c x + \omega_c t) + w_i \cos(k_c x + \omega_c t)) + C$, where C is a real constant. Isovalues are presented over a spatial period $\lambda_c = 2/k_c.\pi$

The linear stability analysis does not give a complete information on the emerging type of flow which can be either standing or traveling waves. The definite answer would require a non-linear analysis. The eigenflows of figures 4 and 5 are solutions of the linear problem for a traveling wave at a given instant and propagating to the left ($\omega_c > 0$, $k_c > 0$). The wave propagating to the right is obtained after a vertical reflection of figures 4–5.

In figure 4 ($S_M \approx S_{M_T}$) from $Le = 10$ to $Le = 1000$ the flow structure and the shape of the isovalues of temperature are relatively insensitive to the Prandtl and Schmidt numbers and the temperature gradients along the free surface remain located in regions where the horizontal component of the velocity is the largest. But we observe important differences in the solute distribution for the three Lewis numbers $Le = 10$, 100 and 1000. For $Le = 10$, isovalues of temperature and concentration have similar shapes in the upper part of the layer. Differences appear in the lower part since boundary conditions along the bottom are different for the two fields. For $Le = 1000$, the concentration isovalues are significantly distorted by the flow compared to those of temperature. In the flow of figure 4–3c ($Le = 1000$), we observe closed iso-lines of concentration which partly follow the streamlines.

In figure 5 ($S_M = -0.5$) and for all cases from $Le = 10$ to $Le = 1000$, the concentration field is much more strongly deformed than in figure 4 ($S_M \approx S_{M_T}$). For $Le = 1000$ (figure 5, cases 3a–c), the concentration isolines fully follow the stream-lines. This phenomenon appears at large Lewis numbers and is enhanced as S_M decreases. As we next discuss, it is part of the mechanism by which the solutal free surface force will have a destabilizing effect on the instability. In the next section, we discuss in detail the combined effect on the instability of the Soret effect (through S_M) and of a mass diffusion less efficient than heat diffusion (large Le).

3.3
The stabilizing solutal contribution as a catalyst for overstability: a physical mechanism

We now propose a physical mechanism that explains the decrease of Ma_c with $|S_M|$ ($S_M < 0$). As we mentioned, the relative positions of the free surface temperature and concentration gradients (i.e. of the driving forces) depend on the three parameters S_M, Pr and Sc and have a key role in the destabilizing effect of the solutal contribution.

To have a better insight into this problem, the variations with the free surface position of the thermally induced surface force $F_T(x) = Pr^{-1}\partial T/\partial x$, the solutally induced part $F_c(x) = S_M\, Pr^{-1}\partial c/\partial x$, and the resulting force $F(x) = F_T(x) + F_c(x) = \partial u/\partial z$ are reported in figure 6 for $Pr = 1$, $Sc = 100$ and $S_M = -10^{-5}$, -10^{-4}, -10^{-3}, -10^{-2} and -10^{-1}. The horizontal component of the velocity u on the free surface has the sign of F (the flow is maintained by viscous diffusion of momentum from the free surface to the fluid) so that the position and size of the rolls can be known from the zeros of F.

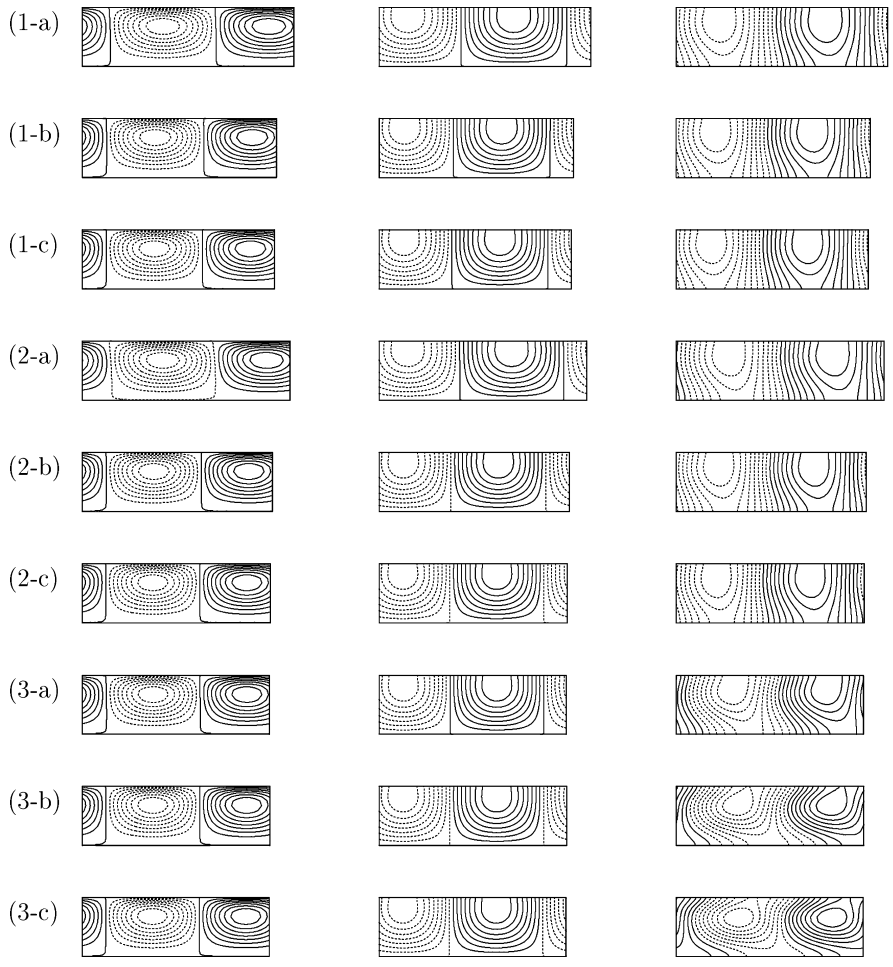

Fig. 4. Isovalues of the stream-function (on the left), temperature and concentration (on the right) of neutral modes for S_M close to S_{M_T}. Isovalues are presented over a period $[0, 2\pi/k_c[$ and at a fixed instant. The flows presented correspond to (1) $Le = 10$ with $(Pr, Sc) = (1 - a)\ (0.1, 1), (1 - b)\ (1, 10)$ et $(1 - c)\ (10, 100)$, (2) $Le = 100$ with $(Pr, Sc) = (2 - a)\ (0.01, 1), (2 - b)\ (0.1, 10)$ et $(2 - c)\ (1, 100)$ (3) $Le = 1000$ with $(Pr, Sc) = (3 - a)\ (0.01, 10), (3 - b)\ (0.1, 100)$ et $(3 - c)\ (1, 1000)$. Solid curves stand for positive isovalues and counter clockwise rolls and dashed lines for negative isovalues and clockwise rolls

For $S_M = -10^{-5}$ (figure 6a) the first bifurcation is steady and we see that the two forces F_T and F_c have exactly opposed signs. This is the signature of the opposite effects of the two contributions: F_T drives the flow whereas F_c brakes it. Note that for such values of S_M, F_c is very small compared to F_T and $F \approx F_T$. This steady case will be used as a reference for which the phase shift between the two forces F and F_c will be set to zero (despite the opposed signs). For larger values of $|S_M|$ corresponding to Hopf bifurcations (figures 6b–e), we observe a displacement of the forces F_T and F_c with respect to F and this displacement increases with $|S_M|$. It is much stronger for F_c than for F_T and creates a phase shift between F_c and F_T. The displacement of F_c with respect to F (and then with respect to u at the free surface) explains the destabilizing effect of the solutal contribution as we next discuss.

Examination of figure 6e shows that the negative contribution of F_c, strictly opposed to F and F_T in the steady case (figure 6a), is now displaced to the right. Therefore, the negative contribution of F_c affects the counter clockwise roll on the right, contributing for this roll to the increase of $|F|$ (as F is also negative) and locally favoring the flow. The different contributions to the surface force are schematically described in figure 7 along the free surface of a clockwise roll. In regions where the fluid rises to the top, both thermal and solutal contributions cooperate to increase the velocity. In contrast, in regions where the fluid descends, the solutal contribution F_c is opposed to the thermal contribution F_T and thus reduces the velocity.

For steady eigenflows (with F_c strictly opposed to F_T), the thresholds increase from Ma_0 with $|F_c|$ and therefore with $|S_M|$. We discussed these cases in subsection 3.1 equating the different contributions to the surface force. In contrast, for the oscillatory cases, the thermal and solutal force distributions along the free surface are not so simple and equating the forces cannot lead to an analytical expression for Ma_c. However, figure 6 clearly shows that the concentration has not the stabilizing effect expected. In a large part of the free surface the concentration and temperature gradients have the same effect on the flow and favor it. In a situation like the one in figure 7 the critical temperature difference required to overcome viscous dissipation, thermal diffusion and the stabilizing solutal contribution may not be larger than that of the pure thermal case. It can decrease with $|S_M|$ from $Ma_c(S_{M_T})$ and can even decrease below Ma_0 in situations as in figure 6e, when the favoring contribution of F_c becomes dominant compared to its braking contribution.

The mechanism that we described is possible at large Lewis number when the concentration isovalues are mainly convected by the flow (see figures 4–5). It is also observed at sufficiently large Marangoni Soret coefficient $|S_M|$ when the solutal surface force has a significant contribution on the total free surface force (figure 6). These

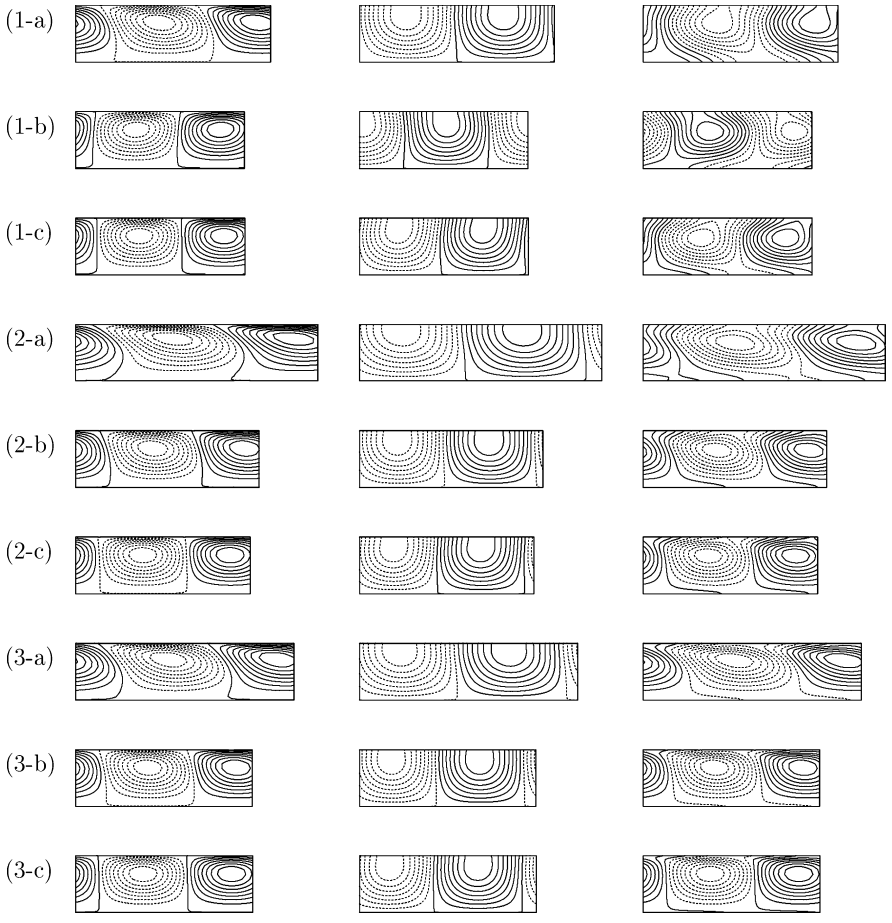

Fig. 5. Isovalues of the stream-function (on the left), temperature and concentration (on the right) of neutral modes for $S_M = -0.5$. Isovalues are presented over a period $[0, 2\pi/k_c[$ and at a fixed instant. The flows presented correspond to (1) $Le = 10$ with $(Pr, Sc) = (1-$ a) (0.1, 1), (1 – b) (1, 10) and (1 – c) (10, 100), (2) $Le = 100$ with $(Pr, Sc) = (2 -$ a) (0.01, 1), (2 – b) (0.1, 10) and (2 – c) (1, 100) (3) $Le = 1000$ with $(Pr, Sc) = (3 -$ a) (0.01, 10), (3 – b) (0.1, 100) and (3 – c) (1, 1000)

observations are in agreement with the results of Chen & Chen [5], Bhattacharjee [6], Skarda et al. [12].

3.4 Bounded boxes

We finally turn our attention to bounded boxes of small aspect ratio. As mentioned by Knobloch & Moore [22], the discontinuity of the curve $\omega_c(S_M)$ disappears in a bounded box due to the constraints produced by the lateral boundaries. This behavior is what we observe in figure 8 where the evolutions of the critical Marangoni number and critical angular frequency with S_M are presented for a bounded box of aspect ratio $A = 2$ with $Sc = 100$ and $Pr = 1$ (only the first bifurcation point is presented despite the fact that for bounded boxes, different flow structures become unstable as the Marangoni number is increased). As $Sc = 100$ and $Pr = 1$, this case corresponds to the situation in which in an infinite layer, Ma_c decays below the critical value for the pure thermal case. This is also what we observe here for a bounded box.

4 Conclusion

Linear analysis of the Marangoni-Bénard instability in binary mixtures subject to Soret effect has been carried out for horizontally infinite fluid layers and two-dimensional boxes. We focused on the onset of oscillatory motions predicted when the thermal contribution to the surface force is destabilizing and the solutal contribution stabilizing (a situation which corresponds to $S_M < 0$ and $Ma > 0$). We computed the critical Marangoni number, wavenumber and angular frequency as functions of the Marangoni Soret parameter S_M for various Prandtl and Schmidt numbers Pr and Sc.

Summarizing the results, we noted that Ma_c decreases for increasing Sc values or decreasing Pr values, that ω_c increases for increasing $|S_M|$ and (in situations with not too small $|S_M|$) for decreasing Pr and Sc.

The main question of this work was to understand why the critical Marangoni number Ma_c of the onset of time periodic motions was a decreasing function of $|S_M|$ for particular choices of (Pr, Sc) [5, 12] since one would expect, from the increase of the stabilizing effect, an increase of the threshold. Observing the flow structure of the critical modes, we noted that for bifurcations to steady state, the temperature and concentration gradients (and thus the forces they generate) have exactly opposed signs, the temperature gradients driving the flow and the concentration gradients braking it. In the oscillatory case, a phase shift appears between the two forces, a phenomenon which is connected to the displacement of the concentration gradients at the free surface. As a consequence, on large regions of the free surface the two forces cooperate to maintain the flow. This phenomenon is the mechanism by which the stabilizing solutal contribution acts as a catalyst for overstability. It appears at large Lewis and at sufficiently large $|S_M|$.

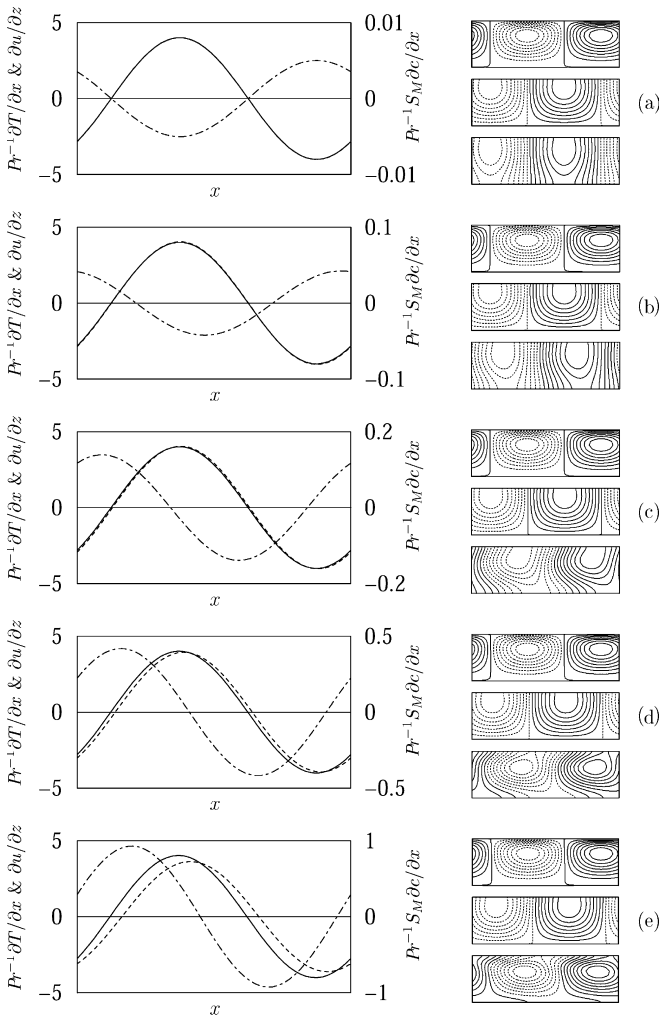

Fig. 6. On the left are presented the thermal contribution to the surface force $F_T(x) = (1/Pr)\ (\partial T/\partial x)$ (dashed curve), the solutal contribution $F_c(x) = (S_M/Pr)\ (\partial c/\partial x)$ (dotted-dashed curve) and the total surface force $F(x) = F_T + F_c = \partial u/\partial z$ (continuous curve) of the critical eigenmode at a given instant t and along the free surface on a spatial period $x \in [0, 2\pi/k_c[$. The values are given within the multiplicative factor k_c. On the right are presented the corresponding critical eigenmodes with on top, isovalues of the streamfunction, in the middle, isovalues of T, and on the bottom, isovalues of c. The situations correspond to $Pr = 1$, $Sc = 100$: (a) $S_M = 10^{-5}$ (steady case for which $\omega_c = 0$ and $Ma_c = 79.70$); (b–e) (oscillatory case for which $\omega_c \neq 0$) with (b) $S_M = 10^{-4}$ ($Ma_c = 80.31$); (c) $S_M = 10^{-3}$ ($Ma_c = 80.25$); (d) $S_M = 10^{-2}$ ($Ma_c = 78.37$); (e) $S_M = 10^{-1}$ ($Ma_c = 73.41$)

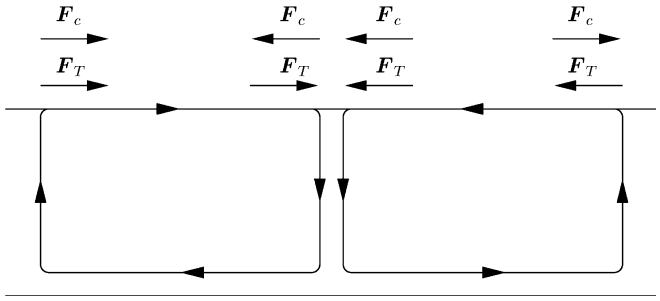

Fig. 7. Sketch of the force distribution along the free surface for a couple of counter rotating rolls

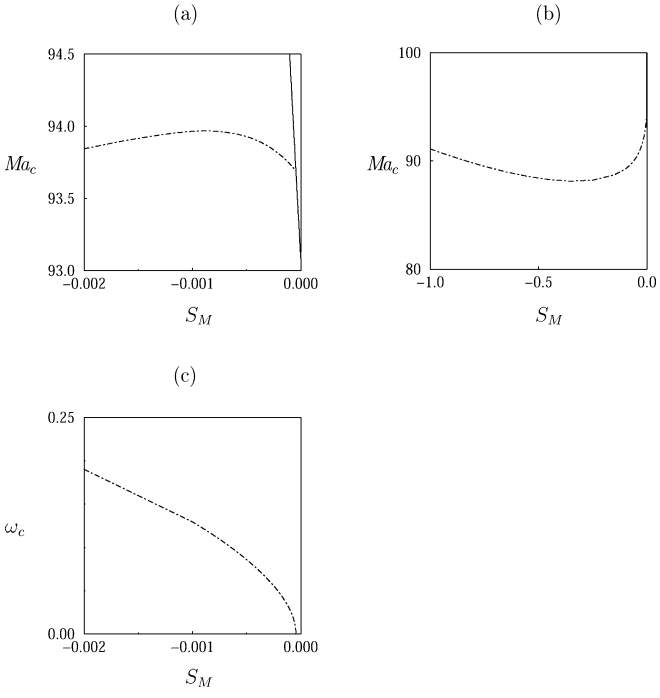

Fig. 8. For a two-dimensional bounded cavity of aspect ratio $A = 2$ and for $Sc = 100$ and $Pr = 1$: evolution of the critical Marangoni number (a, b) and critical pulsation (c) with the Marangoni Soret parameter S_M. Resolution is 15×13

In the last part of this paper, we focused on two-dimensional boxes of finite aspect ratio, $A = 2$. We confirmed the existence of a codimension-two primary bifurcation point below which first primary bifurcations are Hopf bifurcations. We also observed that for $Sc = 100$ and $Pr = 1$, the stabilizing solutal contribution also acts as a catalyst for overstability.

We finally mention that the unexpected destabilizing action of a stabilizing force has yet been observed in other physical situations and explained by Acheson [24]. The author discussed situations in which overstability is enhanced by the addition of a stabilizing force. A typical example is detailed by Net et al. [25] for a binary fluid in a rotating cylinder. In the physical examples discussed by Acheson a key point is the existence of two natural frequencies in the problem. For instance, in the problem considered by Net et al., one frequency comes from the Hopf bifurcation created via the Soret effect and an other from the rotation of the cylinder. The mechanism that we discussed here is basically different.

Appendix A

In the following, and for simplicity we drop the star from the notation and denote with the subscripts r and i the real and imaginary parts of the unknown functions respectively. Replacing the expansion of the variables into the linearized equations and identifying the real and imaginary parts of the resulting set of equations, we get the following ordinary differential equations:

$$
\begin{aligned}
&u_r'' - k^2 u_r + k p_i = -\omega u_i,\\
&u_i'' - k^2 u_i - k p_r = \omega u_r,\\
&w_r'' - k^2 w_r - p_r' = -\omega w_i,\\
&w_i'' - k^2 w_i - p_i' = \omega w_r,\\
&-k u_i + w_r' = 0,\\
&k u_r + w_i' = 0,\\
&-Ma\, w_r + Pr^{-1}(T_r'' - k^2 T_r) = -\omega T_i,\\
&-Ma\, w_i + Pr^{-1}(T_i'' - k^2 T_i) = \omega T_r,\\
&-Ma\, w_r + Sc^{-1}(c_r'' - T_r'' - k^2(c_r - T_r)) = -\omega c_i,\\
&-Ma\, w_i + Sc^{-1}(c_i'' - T_i'' - k^2(c_i - T_i)) = \omega c_r,
\end{aligned}
$$

along with the boundary conditions:

$$
\begin{aligned}
&u_r'(1) + Pr^{-1}k(T_i(1) + S_M c_i(1))\\
&\quad = u_i'(1) - Pr^{-1}k(T_r(1) + S_M c_r(1)) = u_r(0) = u_i(0) = 0,
\end{aligned}
$$

$$
w_r(1) = w_i(1) = w_r(0) = w_i(0) = 0,
$$

$$
\begin{aligned}
p_r'(1) + k^2 w_r(1) - w_r(1) &= p_i'(1) + k^2 w_i(1) - w_i''(1)\\
&= p_r'(0) + k^2 w_r(0) - w_r''(0)\\
&= p_i'(0) + k^2 w_i(0) - w_i''(0) = 0,
\end{aligned}
$$

$$
T_r(0) = T_i(0) = T_r'(1) = T_i'(1) = 0,
$$

$$
\begin{aligned}
T_r'(0) - c_r'(0) &= T_i'(0) - c_i'(0) = T_r'(1) - c_r'(1)\\
&= T_i'(1) - c_i'(1) = 0.
\end{aligned}
$$

References

1. Castillo, J.L. & Velarde, M.G.: Thermal diffusion and the Marangoni instability of a two component fluid layer heated from below.: Phys. Letters 66A (1978) 489–491
2. Castillo, J.L. & Velarde, M.G.: Buoyancy-thermocapillary instability: The role of interfacial deformation in one- and two-component fluid layers heated from below or above. J. Fluid Mech. 125 (1982) 463–474
3. Van Vaerenbergh, S., Colinet, P., Georis, Ph. & Legros, J.C.: Preparatory results for a Marangoni-Bénard experiment with Soret effect in micro-gravity conditions. Unpublished (1991)
4. Henry, D., Ben Hadid, H., Van Vaerenbergh, S., Legros, J.C. & Roux, B.: Marangoni-Bénard instabilities in liquid mixtures with Soret effect. Proceedings of the VIIIth European Symposium on Materials and Fluid Sciences in Microgravity ESA SP 333 (1992) 717–721
5. Chen, C.F. & Chen, C.C.: Effect of surface tension on the stability of a binary fluid layer under reduced gravity. Phys. Fluids 6 (1994) 1482–1490
6. Bhattacharjee J.K.: Marangoni convection in binary liquids. Phys. Rev. E 50 2 (1994) 1198–1204
7. Joo, S.C.: Marangoni instabilities in liquid mixtures with Soret effects. J. Fluid Mech 293 (1995) 127–145
8. Bergeon, A., Henry, D. & BenHadid, H.: Marangoni-Bénard instability in microgravity conditions with Soret effect. Int. J. Heat Mass Transfer 37 (1994) 1545–1562
9. Bergeon, A., Henry, D., BenHadid, H. & Tuckerman, L.S.: Stability analysis of Marangoni convection in binary mixtures subjected to the Soret effect. ASME HTD 290 (1994) 63–69
10. Bergeon, A., Henry, D. & BenHadid, H.: Analytical linear stability analysis of Marangoni instability with Soret effect. Microgravity Quarterly 5 (1995) 123–129
11. Bergeon, A., Henry, D., BenHadid, H. & Tuckerman, L.S.: Marangoni convection in binary mixtures with Soret effect. J. Fluid Mech. 375 (1998) 143–177
12. Skarda, J.R.L., Jacqmin, D. & McCaughan, F.E.: Exact and approximate solutions to the double-diffusive Marangoni-Bénard problem with cross-diffusive terms. J. Fluid Mech. 366 (1998) 109–133
13. Slavtchev, S., Simeonov, G., Van Vaerenbergh, S. & Legros, J.C.: Marangoni instability of a layer of binary liquid in the presence of nonlinear Soret effect. Int. J. Heat Mass Transfer 42 15 (1999) 3007–3011
14. Pearson, J.R.A.: On convection cells induced by surface tension. J. Fluid Mech. 4 (1958) 489–500
15. De Groot, S.R. & Mazur, P.: Non Equilibrium thermodynamics. North Holland, Amsterdam, 1969
16. Kolodner, P., Williams, H. & Moe, C.: Optical measurement of the Soret coefficient of ethanol/water solution. J. Chem. Phys. 88 (1988) 6512
17. Seydel, R.: Pratical Bifurcation and Stability Analysis. From equilibrium to chaos. Interdisciplinary Applied Mathematics 5 IAM, Springer-Verlag, 1994
18. Funaro, D.: Polynomial approximation of differential equations. Lecture notes in Physics m8, Springer-Verlag, 1991
19. Bernardi, C. & Maday, Y.: Approximations spectrales de problèmes aux limites elliptiques. Mathématiques & Applications 10, Springer-Verlag, 1992
20. Tuckerman, L.S.: Steady-state solving via Stokes preconditioning; Recursion relations for elliptic operators. In Proceedings of the 11th International Conference on Numerical Methods in Fluid Dynamics, edited by D.L. Dwoyer, M.Y. Hussaini & R.G. Voigt, Springer-Verlag, 1989
21. Mamun, C.K. & Tuckerman, L.S.: Asymmetry and Hopf bifurcation in spherical Couette flow. Phys. Fluids 7 (1995) 80–91
22. Knobloch, E. & Moore, D.R.: Linear stability analysis of experimental Soret convection. Phys. Rev. A. 37 (1988) 860–870
23. Henry, D. & Roux, B.: Soret separation in a quasi-vertical cylinder. J. Fluid Mech. 195 (1988) 175–200
24. Acheson, D.J.: Stable density stratification as a catalyst for instability. J. Fluid Mech 96, 723–733, 1980
25. Net, M., Mercader, I. & Knobloch, E.: Binary fluid convection in a rotating cylinder. Phys. Fluids 7 (1995) 1553–1567